HHS Public Access

Author manuscript

Phys Med Biol. Author manuscript; available in PMC 2016 September 07.

Published in final edited form as:

Phys Med Biol. 2015 September 7; 60(17): 6751–6773. doi:10.1088/0031-9155/60/17/6751.

Anatomical-based Partial Volume Correction for Low-dose Dedicated Cardiac SPECT/CT

Hui Liu[1,2], **Chung Chan**[1], **Yariv Grobshtein**[3], **Tianyu Ma**[2], **Yaqiang Liu**[2], **Shi Wang**[2], **Mitchel R. Stacy**[4], **Albert J. Sinusas**[1,4], and **Chi Liu**[1]

Chi Liu: chi.liu@yale.edu

[1]Department of Diagnostic Radiology, Yale University, New Haven, CT, 06511, USA

[2]Key Laboratory of Particle & Radiation Imaging (Tsinghua University), Ministry of Education, Beijing, 100084, China

[3]GE Healthcare, Haifa, 34384, Israel

[4]Yale Translational Research Imaging Center, Department of Internal Medicine, Yale University, New Haven, CT, 06511, USA

Abstract

Due to the limited spatial resolution, partial volume effect (PVE) has been a major degrading factor on quantitative accuracy in emission tomography systems. This study aims to investigate the performance of several anatomical-based partial volume correction (PVC) methods for a dedicated cardiac SPECT/CT system (GE Discovery NM/CT 570c) with focused field-of-view (FOV) over a clinically relevant range of high and low count levels for two different radiotracer distributions. These PVC methods include perturbation Geometry Transfer Matrix (pGTM), pGTM followed by multi-target correction (MTC), pGTM with known concentration in blood pool, the former followed by MTC and our newly proposed methods, which perform the MTC method iteratively, where the mean values in all regions are estimated and updated by the MTC-corrected images each time in the iterative process. The NCAT phantom was simulated for cardiovascular imaging with ^{99m}Tc-tetrofosmin, a myocardial perfusion agent, and ^{99m}Tc-red blood cell (RBC), a pure intravascular imaging agent. Images were acquired at six different count levels to investigate the performance of PVC methods in both high and low count levels for low-dose applications. We performed two large animal *in vivo* cardiac imaging experiments following injection of ^{99m}Tc-RBC for evaluation of intramyocardial blood volume (IMBV). The simulation results showed our proposed iterative methods provide superior performance than other existing PVC methods in terms of image quality, quantitative accuracy, and reproducibility (standard deviation), particularly for low-count data. The iterative approaches are robust for both ^{99m}Tc-tetrofosmin perfusion imaging and ^{99m}Tc-RBC imaging of IMBV and blood pool activity even at low count levels. The animal study results indicated the effectiveness of PVC to correct the overestimation of IMBV due to blood pool contamination. In conclusion, the iterative PVC methods can achieve more accurate quantification, particularly for low count cardiac SPECT studies, typically obtained from low-dose protocols, gated studies, and dynamic applications.

Keywords

Anatomical-based PVC; iterative MTC; low-dose cardiac SPECT

1. Introduction

Although state-of-the-art emission tomography systems have improved spatial resolution (Garcia *et al.*, 2011; Wienhard *et al.*, 2002), partial volume effect (PVE) remains a major factor that limits the quantitative accuracy, particularly for small objects. PVE generally is due to two factors. First, due to limited system resolution and post-reconstruction smoothing, each voxel could suffer from a combination of spill-in effects from adjacent voxels causing overestimation, and spill-out effects causing underestimation. Second, since image voxel size is finite, each voxel can contain more than one tissue with different tracer concentrations, thus limiting quantitative accuracy (Erlandsson *et al.*, 2012).

In practical emission tomography applications, the spatially variant resolution can lead to spatially variant PVE and quantitative errors. In cardiac imaging, the thickness of the myocardium changes across the cardiac cycle, leading to cycle-dependent PVE. Additionally, respiratory motion and body motion could also introduce PVE. In dynamic cardiac PET and SPECT studies, the relative effects between spill-in and spill-out could change over time as blood pool has higher tracer concentration than that of myocardium in early phases and vice versa in later phases. In longitudinal PET studies that evaluate responses to cancer therapy, tumor size and shape often change over time, resulting in temporal dependent PVE. In such cases, performing partial volume correction (PVC) is critical for achieving accurate quantitative assessments.

Various partial volume correction methods have been proposed. A comprehensive review of these methods can be found in (Erlandsson *et al.*, 2012). With the advent of hybrid imaging such as SPECT/CT and PET/CT, both functional and anatomical images are acquired within one imaging session with close alignment. Anatomical-based PVC methods are particularly promising for hybrid scanners, as various regions could be segmented into several templates accurately from anatomical images. For various existing multi-region anatomical-based PVC methods, including geometric transfer matrix (GTM) (Rousset *et al.*, 1998), perturbation GTM (pGTM) (Du *et al.*, 2005), Muller-Gartner method (MGM) (Muller-Gartner *et al.*, 1992), Yang method (Yang *et al.*, 1996a), multi-target correction (MTC) (Erlandsson *et al.*, 2006) and region-based voxel-wise correction (RBV) (Thomas *et al.*, 2011), both spill-in and spill-out contamination among different regions could be taken into account during compensation. Among them, some PVC approaches only correct the mean values of regional concentrations, such as GTM and pGTM, while other approaches could correct the entire image on a voxel-by-voxel basis, such as MGM, MTC, Yang method and RBV.

All these methods require the segmentation of several regions employing separately, sequentially or simultaneously acquired anatomical images to generate templates, the registration of functional and anatomical images, and the calculation of the regions template responses in the imaging system. With the template response, the cross-talk factors (spill-in, spill-out) among regions that are responsible for the PVE could be determined for subsequent PVC. Typically, there are two methods to determine the template's response. One method is to forward project and reconstruct the binary template with realistic depth

dependent collimator-detector response for SPECT systems and spatially variant Point Spread Functions (PSF) for PET systems. The other method is to convolve the template with image-based PSF. Both methods could provide spill-in and spill-out factors in all the regions for subsequent PVC with no substantial difference (Frouin *et al.*, 2002; Soret *et al.*, 2003).

Among the typical anatomical-based PVC methods, GTM and pGTM only calculate the mean value of the templates' response in each region to compose the geometry transform matrix. The corrected mean value of each region could be obtained through a matrix inverse operation (Du *et al.*, 2005; Rousset *et al.*, 1998). The MGM method corrects both spill-in effect and spill-out effect voxel-by-voxel for only one target region by subtracting spill-in effect from other regions and dividing the spill-out factor. The spill-in effect is estimated by templates' response of surrounding regions multiplied by the known estimation of surrounding regions' mean values. The spill-out factor is obtained from the target region's template response (Muller-Gartner *et al.*, 1992). The Yang method obtains the correction factor from one single template response while the template is composed of several templates of different regions, each weighted by the prior knowledge of known concentration ratios (Yang *et al.*, 1996a).

The MTC method is an extension of MGM. It is applied successively on each region in turn using the mean value estimation in all regions obtained from GTM (Erlandsson *et al.*, 2006). Additionally, the RBV correction method is similar to the Yang method except that regional mean values are initially obtained with GTM (Thomas *et al.*, 2011).

In current SPECT/CT and PET/CT applications, dose-reduction is gaining interest. With a decrease in injected dose, the image noise would be increased. To our knowledge, the performance of various PVC methods for low-counts data have not been comprehensively investigated for cardiac SPECT applications. Considering most existing PVC methods would amplify image noise (Hoetjes *et al.*, 2010), investigation for low-counts data is also important for applications of respiratory and/or cardiac gating, and dynamic SPECT studies with tracer kinetic modeling, where only a fraction of counts are used to generate image frames with higher noise.

Different tracer distributions may have different partial volume degradation effects and PVC methods may perform differently for various tracers. When the myocardium is the organ of interest for quantification purposes, typical myocardial perfusion tracers lead to higher uptake in the myocardium than that in the blood pool, while blood pool tracers lead to higher uptake in the blood pool than that in the myocardium. In dynamic SPECT and PET, the ratio of myocardium to blood pool concentration is more complicated and changes over time. Thus, investigation of various PVC methods for different tracer distributions is critical.

Compared to conventional SPECT, recent state-of-the-art dedicated cardiac SPECT systems typically focus the imaging geometry to the heart, leading to a smaller field-of-view (FOV). For organs outside of the FOV, there may be insufficient projection angles to provide fully 3D complete angle reconstruction. Due to the incompleteness of projection data, inaccurate quantification of organs outside of the FOV may indirectly affect the quantification of PVC results for organs inside the FOV, as the mean activities of regions both inside and outside

FOV are used for spill-in correction in many PVC methods. However, little work on PVC has been performed on small FOV systems, as most PVC methods were applied on the large FOV SPECT and PET imaging scanners. The issue of PVC is further complicated when performing cardiac imaging on a small FOV system due to the additional confounding issue of cardiac and respiratory motion.

To address the gaps outlined above, this study focuses on investigating the performance of various existing anatomical-based PVC methods and our newly proposed PVC methods for a dedicated cardiac SPECT/CT system (GE Discovery NM/CT 570c) with low count cardiac image data for two different tracer distributions. Our proposed PVC approaches perform MTC method iteratively, while the mean values in all regions are estimated and updated by the MTC-corrected images each time in the iterative process. The NCAT phantom was used to simulate cardiovascular imaging with two ^{99m}Tc-labeled tracers; ^{99m}Tc-tetrofosmin, a myocardial perfusion agent, and ^{99m}Tc-red blood cell (RBC), a pure intravascular imaging agent. Data were simulated for both radiotracers, at six different count levels to address the critical issue of signal to noise associated with PVC. We also evaluated data acquired from two large animal *in vivo* cardiac imaging experiments following injection of ^{99m}Tc-RBC for evaluation of intramyocardial blood volume.

2. Materials and methods

2.1 Phantom Simulations

In this study, we simulated two SPECT tracer distributions using the NCAT phantom (Segars *et al.*, 2000). The first radiotracer distribution simulated was ^{99m}Tc-tetrofosmin, an agent commonly used for SPECT myocardial perfusion imaging (MPI). A perfusion defect at lateral location in the short axis view with a size of 60° radial range and 1 cm axial length was created as shown in Figure 1 (He *et al.*, 2004). The tracer's relative concentration ratios in normal myocardium, perfusion defect, blood pool, liver, lung and background were set to 100, 50, 10, 50, 5 and 10, respectively, as shown in Figure 1. With the myocardium as the organ of interest, the dominant partial volume effect for this tracer is "spill-out" from the myocardium to the blood pool at the typical time points for myocardial perfusion imaging. In typical contrast enhanced cardiac CT, the exact boundary between perfusion defect and normal myocardium is not visible. Therefore, the anatomical information derived from contrast CT in this simulation study did not contain the boundary of defect, but only the endocardium and epicardium surfaces as shown in Figure 1 (bottom row). In this case, we are particularly interested in the performance of partial volume correction for the defect region without the exact boundary of the defects from anatomical images.

The second simulated radiotracer was ^{99m}Tc-labeled red blood cells (^{99m}Tc-RBC), which can be used to quantify regional and global left ventricular function as well as intramyocardial blood volume (IMBV), defined as the fraction of myocardium that is occupied by blood. This radiotracer represents a promising agent that could be used to assess the microvascular circulation within the myocardium, in terms of the evaluation of IMBV. The IMBV can be quantified as the activity in the myocardium divided by the activity in the blood pool (Liu *et al.*, 2013). In the simulation, the relative tracer concentration ratios in myocardium, blood pool, liver, lung and background were set to 15, 100, 15, 2 and 1,

respectively, illustrated in Figure 1 (middle row), leading to a 15% IMBV, which is typical for normal human and large animals. Since the uptake is higher in the blood pool than in the myocardium for this tracer, the partial volume effect for myocardium is dominated by the "spill-in" effect from blood pool and other organs into the myocardium.

2.2. SPECT system and reconstruction

We simulated a dedicated cardiac hybrid SPECT/CT imaging system (GE Discovery NM/CT 570c SPECT/CT system) with 19 solid-state CZT pixelated detectors and focused pinhole collimators (Bocher *et al.*, 2010). All 19 detectors are distributed in 3 rows, over an approximate 180° arc with the pinhole collimators focused on a small FOV (~19 cm in diameter) that covers the entire heart, providing stationary data acquisition geometry. Different from conventional SPECT systems with parallel-hole collimators, only a limited FOV can be fully reconstructed with sufficient projection views. The spatial resolution of this system reported varied between 5 mm and 9 mm inside the FOV (Kennedy *et al.*, 2014). This hybrid SPECT/CT system incorporates a diagnostic 64-slice CT scanner that can provide co-registered non-contrast CT image for attenuation correction and contrast-enhanced CT image for partial volume correction.

The projection data of NCAT phantom were simulated including the effects of attenuation and collimator-detector response. The noise-free projections (shown in Figure 2) were acquired by forward-projecting the NCAT phantom with a pre-calculated system matrix, including the effects of collimator-detector responses. This system matrix was identical to the one used by the camera for routine clinical studies. The noisy projections were generated based on Poisson distribution. To evaluate the performance of partial volume correction on low-count data, we simulated 5 noise levels. The corresponding total counts in the projection for each level were $8e^6$, $5e^6$, $2e^6$, $1e^6$ and $5e^5$ respectively. This range of count density was relevant to the typical *in vivo* acquisition, which yielded a $2e^6$ count level for a 1 min acquisition based on a dog study following injection of 24 mCi ^{99m}Tc-RBCs in the next section. For each noise level, 50 independent noise realizations were generated to calculate the mean and the standard derivation images.

MLEM method was used to reconstruct all projection data with 80 iterations without post-reconstruction filter. The images were reconstructed using the same system matrix used in the simulations with voxel dimension of 4 mm. Image reconstructions were optimized using CT-derived body contours and attenuation correction as previously reported by our group for quantitative image analysis (Chan *et al.*, 2012).

2.3. Animals studies

One dog (23.6 kg) and one pig (20 kg) were imaged using a hybrid SPECT/CT system (GE Discovery NM/CT 570c) following intravenous injection of ^{99m}Tc-RBCs (885.6±48.9 Mbq). The pig was sedated with intramuscular ketamine (22 mg/kg) and xylazine (5 mg/kg), and the dog was sedated via peripheral intravenous propofol (7–7.5 mg/kg). Both animals were intubated and mechanically ventilated (Venturi; Cardiopulmonary Corp, Milford, CT) with 35% oxygen, 65% nitrous oxide, and 1% to 3% isoflurane. Blood pressure, oxygen saturation, and ECG signal were continuously monitored during all imaging acquisitions

(IntelliVue MP50; Philips Healthcare, Andover, MA). A 5-F polyethylene catheter was placed in the jugular vein for administration of fluids, CT contrast agent, and radioisotope. Prior to imaging, animals underwent a thoracotomy for visualization of the heart as part of an additional set of experiments not outlined in the present work. All pre-clinical SPECT data were acquired in list-mode over 15 minutes. In the dog study, the list-mode data of 10 minutes (5–15 min post-injection to eliminate early dynamic tracer distribution changes in the first 5 min) were considered as high counts case. We then included only the first 2 seconds data of the 10 min dataset (i.e. starting 5 min after injection) and rebinned to generate the projection data as low counts case for reconstruction and partial volume correction. Our goal here was not to match the count level of animal study with computer simulation, but to demonstrate our proposed PVC methods are more robust than conventional PVC methods in low count studies, using an extremely low count level as an example.

Non-contrast CT data were acquired for attenuation correction and contrast-enhanced CT data were acquired to guide PVC. All X-ray cineCT data were acquired retrospectively with ECG gating during the end-expiration respiratory phase by temporarily disconnecting the ventilator. The non-contrast CT scans for attenuation correction were acquired at 120 kVp, 20 mA, with pitch of 0.97:1, slice thickness of 5 mm, and rotation speed of 0.8 secs, and reconstructed using filtered back projection. The contrast CT images were acquired at 120 kVp, 35 mA, with pitch of 0.24:1, slice thickness of 0.625 mm, and rotations speed of 0.35 secs. The contrast CT images were reconstructed using filtered back projection from the end-diastolic phase (70% RR interval) in the dog study, and reconstructed with a voxel size of 0.625 mm. In the pig study, both SPECT and contrast CT data were reconstructed for 8 phases of the cardiac cycle, so the PVC could be applied for each gated reconstruction with matched contrast CT data. All experimental protocols were approved by the Institutional Animal Care and Use Committees and were in compliance with the Association for Assessment and Accreditation of Laboratory Animal Care International policies.

2.4. PVC Methods

As described below, we implemented several anatomical-based PVC methods and proposed a new iterative PVC approach here, based on the combination of pGTM (Du *et al.*, 2005) and MTC (Erlandsson *et al.*, 2006) for partial volume correction. All methods required the four steps of segmentation of contrast CT images to generate templates for each region/organ, registration between SPECT and CT images, generation of template response, and correction for PVE.

2.4.1. Segmentation and registration—For PVC, the regions' templates with tissue fraction were obtained from the segmentation of high-resolution contrast CT images. The difference between templates with and without tissue fraction was at the boundary of adjacent regions. Previous studies have demonstrated that the templates with tissue fractions would improve the quantitative accuracy of PVC (Pretorius and King, 2008). In this study, we first performed the segmentation based on CT images reconstructed with 0.625 mm voxels. Then we down sampled the segmented templates to match SPECT voxel size of 4 mm, t o create templates with tissue fractions.

In both simulation and animal studies, we segmented and generated five region templates including myocardium, blood pool, liver, lung, and the background. For the open-chest dog study, there was bleeding into the chest cavity, therefore an additional region was defined for ^{99m}Tc-RBC that had pooled in the chest cavity.

In the simulation, the templates for each region of NCAT phantom were accurately registered and accounted for the tissue fraction through segmentation of NCAT phantom with different voxel sizes. The CT images aligned with SPECT images perfectly allowing us to eliminate the possible confounding errors from segmentation and registration steps. Figure 3 shows sample slices of the templates containing myocardium, blood pool, lung and liver in different views, after down sampling. The gradient in the images represents tissue fraction factors. It can be seen that the voxels at the region boundary were in gradient color, indicating those voxels contained two or more anatomical regions.

Since the perfusion defect was not visible in the contrast CT images in our simulation, the perfusion defect and normal myocardium (excluding defect) were segmented into one single template. To evaluate the performance of these PVC methods in the presence of a perfusion defect, the ROIs of the perfusion defect and normal myocardium can be identified from the original NCAT phantom.

In both animal studies, all the region templates were obtained from the high-resolution contrast CT images. After segmentation, the templates were rigidly registered with the SPECT images, including translation and rotation, and then down sampled to match with SPECT resolution to account for tissue fraction.

2.4.2. Generation of templates response—For PVC, the response of each region template, which could be assumed as the regional cross talk factors among different regions, was calculated as described in (Du *et al.*, 2005). The segmented binary templates were first forward projected and then the projection of the templates were reconstructed to generate the template response using the same perturbation method as described in (Du *et al.*, 2005). In this study, we adopted 0.01 as the perturbation term according to pilot simulation studies.

2.4.3. PVC approaches—In this study, we investigated six anatomical-based PVC approaches, which can be considered as combinations of various implementations of region-based pGTM and voxel-wise MTC. These methods are summarized in Table 1 below.

Methods A and B were two conventional PVC approaches. Due to the sensitivity of blood counting, Methods C and D were only applicable to the radiotracers where the blood concentration was high enough at the equilibrium state. So in this study, methods C and D were only applied to the RBC data. The only difference between our proposed Methods E and F was the initial value input for iterative MTC. Method F used pGTM to estimate the mean activity in each region while Method E was applied directly on the MLEM reconstructed images without the prior pGTM step to calculate the mean activity as the initial estimation. The simulation studies showed the iterative MTC (methods E and F) results have little change (less than 1% change in the mean activity) after 3–4 iterations. Therefore, we used 5 iterations throughout this study.

For all voxel-based PVC methods in Table 1, both spill-in and spill-out effects are corrected for each region. The general framework is described below. With the estimated mean value of each region, the voxel-based correction is applied on all voxels in each region first, as shown in Eq.1. Subsequently, the corrected image of each region is patched together, as shown in Eq.2.

$$f(ROI_i)=\frac{(\mathrm{R}(\mathrm{Pm})*ROI_i-\sum_{j\neq i}EM_j*\mathrm{R}(\mathrm{P}(T_j)))*ROI_i)}{\frac{\mathrm{R}(\mathrm{P}(T_i))}{T_i}*ROI_i} \quad \text{Eq. 1}$$

$$f=\sum_i f(ROI_i) \quad \text{Eq. 2}$$

where ROI_i represents the i^{th} region of interest (ROI). (Pm) is the reconstructed image from the measured projection, Pm. EM_j is the estimated mean value of the j^{th} region. T_j is the j^{th} tissue template. R(P(T_j)) is the j^{th} tissue template reconstruction using the perturbation approach (Du *et al.*, 2005). $f(ROI_i)$ is the i^{th} region image after voxel-based partial volume correction, and f is the final corrected image by patching PVC images of all regions together. For pGTM approach, the voxel-based correction was skipped and the implementation was identical to that in (Du *et al.*, 2005).

2.5. Evaluation

2.5.1. Simulation—For both MPI and RBC simulations, the normalized bias of mean images and standard deviation images derived from 50 noise realizations were calculated to evaluate different PVC approaches. The normalized bias was calculated by subtracting the ground truth NCAT phantom image from mean images and being divided by true NCAT images on a voxel-by-voxel basis, as shown in Eq.3.

$$f^i_{Bias}=\frac{\tilde{f}^i-f^i_{True}}{f^i_{True}}\times 100\% \quad \text{Eq. 3}$$

where f^i_{Bias} is the normalized bias of the i^{th} voxel. $\tilde{f_i}$ is the i^{th} voxel of the mean image from 50 realizations. f^i_{True} is the i^{th} voxel of the true phantom image. The normalized bias images were visually evaluated to compare the accuracy of the PVC approaches.

The standard deviation images were obtained by calculating voxel-by-voxel standard deviation across 50 noise realization images to evaluate the voxel-to-voxel variation.

To evaluate the performance of the PVC approaches on myocardium with defect but without the exact defect boundary in CT, the normalized bias of mean concentrations in normal myocardium, perfusion defect and the contrast ratio between myocardium and defect (the myocardium-to-defect contrast) were calculated for each noise realization in the MPI simulation. The ROIs defining the normal myocardium and perfusion defect were determined based on the NCAT phantom. Further, mean and standard deviation of the bias were acquired with 50 realizations.

In the simulation of RBC tracer, IMBV was estimated as:

$$IMBV = C_m / C_b \quad \text{Eq. 4}$$

where C_m is the ^{99m}Tc-RBC tracer concentration in the myocardium and C_b is the tracer concentration in the blood pool. C_m can be calculated either in the entire heart for global IMBV or on voxel basis. The mean and standard derivation of IMBV bias across 50 noise realizations were also determined.

2.5.2. Animal Studies—In both the dog and pig studies, IMBV values were calculated. In the gated pig study, the variability of mean activities of blood pool across all cardiac gates were also determined to investigate the impact of partial volume correction on improving the quantification consistency across gates.

3. Results

3.1. NCAT Phantom Study

As Methods A and C (pGTM without and with known blood pool concentration) only provided corrected regional mean values and could not generate a new PVC corrected image voxel-by-voxel, Figures 4 – 9 did not include the PVC results of Methods A and C.

As ^{99m}Tc-tetrofosmin simulation results shown in Figure 4, at the higher count levels, there were no substantial differences among the results from different PVC approaches. However, at the lower count levels, the artifacts appeared as a signal void in the right ventricle as denoted by the white arrows in PVC images with method B (pGTM+MTC), due to inaccurate estimation of regional mean concentrations derived from the pGTM method in high noise data. Methods E (iMTC) and F (pGTM+iMTC) provided similar images with fewer artifacts as compared to images of Method B (pGTM+MTC). As compared to no PVC results, the defect definition was visually improved using Methods E and F. While pGTM could provide inaccurate mean region estimations (more than 50% bias, depending on the noise level) for high noise data, pGTM+iMTC method robustly generated PVC images with fewer artifacts. Despite these, speckle noise was visible due to the fact that the correction factors were derived from perturbation approach, which was directly related to the noisy projection. Figure 5 shows the sample slices for ^{99m}Tc-RBC simulation. Similar to results in Figure 4, PVC methods with iterative MTC (iMTC), both without and with pGTM as the initial estimation (the last two columns), gave similar results at low noise levels and images with less artifacts at high noise levels, as compared to the results of pGTM+MTC. It could be observed that with known blood pool concentration as *a priori*, pGTM+MTC provides similar results as the two iterative MTC methods in the last two columns.

As demonstrated by the bias images of ^{99m}Tc-tetrofosmin simulation shown in Figure 6, without PVC for all the count levels, the myocardium was underestimated due to the “spill-out” effect and the blood pool was overestimated. The overestimation was prominent particularly for the regions close to the myocardium, due to the “spill-in” counts from myocardium. In Figure 6, all three PVC methods provided almost identical bias images with reduced bias compared with the one without PVC for noise-free simulation. However, at

lower count levels, the Method B (pGTM followed by MTC) yielded progressively inferior results with substantial underestimation in the lung and blood pool, likely due to the overcorrection caused by inaccurate region mean estimations from pGTM. For the $5e^5$ counts case, the artifacts in the images were too severe to recognize the shape of the myocardium. In contrast, the proposed iterative PVC methods both without and with pGTM as the first step yielded consistent mean images with low bias across all count levels, with slightly more artifacts at lower count levels. Similar observations were found in Figure 7, where all PVC methods provided nearly uniform bias images in the noise-free simulation. The Method B (pGTM followed by MTC) yielded progressively inferior results in low count data. Again, our proposed iterative PVC methods yielded consistent mean images with low bias. With known blood pool concentration, the pGTM+MTC method also yielded mean images with lower bias in myocardium than the pGTM+MTC method without known blood pool concentration. For high count data, the mean images in Figure 7 were more uniform than those in Figure 6 for the two iterative MTC methods, indicating these methods might be more effective for applications with ^{99m}Tc-RBC tracer than for ^{99m}Tc-tetrofosmin.

The trend on image noise as reflected by the standard deviation images shown in Figures 8 and 9 were similar to the trend of the bias images for both tracers. With low noise levels, all PVC methods provided similar standard deviation images. While for high noise cases, the method of pGTM+MTC substantially amplified image noise as reflected by the high standard deviations while the proposed iterative MTC methods and the method with known blood pool concentrations effectively controlled image noise. However, the noise levels with PVC were still higher than the noise level in no PVC image.

As shown in Figure 10 (a) – (b), without PVC, the ROI mean activities were underestimated in both the normal myocardium and the defect. All PVC methods led to reduced bias in noise-free and low noise data. Method B (pGTM followed by MTC) appeared to be more sensitive to noise and resulted in larger bias and standard deviation for low count data. The iMTC method yielded more consistent bias across all noise levels, except for the highest noise level. The pGTM+iMTC method yielded similar results as the iMTC method in terms of mean and standard deviation, except for higher standard deviations in both myocardium and defect for the lowest count level, due to the use of the pGTM results with large standard deviation as the initial value. This demonstrated the robustness of iMTC to low counts data. As shown in Figure 10 (c), the normalized bias of the myocardium-to-defect contrast of the PVC results generated with Method E (iMTC) was smaller than that with Method B (pGTM followed by MTC). However all the PVC methods yielded higher normalized bias than the no PVC results. This was due to the fact that the spill-out effect from the defect into blood-pool and lung was corrected, while the spill-in effect from the normal myocardium into the defect was not corrected due to the missing anatomical boundaries in the template. Consequently, the partial PVC on the defect region yielded moderate over estimation and thus reduced contrast.

In the Tc^{99m}-RBC simulations, the true IMBV was 15%. As shown in Figure 10 (d), for the 50 noise realization results, without PVC, the IMBV was 22%, which was over-estimated by nearly 40% relatively for the entire myocardium. IMBV was accurately corrected to the true level for noise-free data using all PVC approaches. With higher noise levels, the

conventional methods of pGTM and the pGTM+MTC (Methods A and B) led to underestimated IMBV with larger standard deviations, except that Method B under-corrected and led to overestimated IMBV for the lowest count data. In contrast, methods using iterative MTC and methods with known blood pool concentration (Methods C–F) all led to accurate quantification with smaller standard deviations. For the counts levels below $1e^6$ counts, the last three methods led to slight underestimation, where the pGTM+iMTC method (Method F) resulted in slightly larger underestimation and standard deviation than Methods C–E.

3.2 Animals studies

As illustrated in the high-count dog study shown in Figure 11, all PVC methods improved the boundary definition of myocardium and blood pool, as denoted by the white arrows. The corresponding IMBV values were reduced from 0.24 without PVC to 0.16, 0.17 and 0.17 with three PVC methods, respectively. For this dataset with high-count level, pGTM+MTC method appeared to provide similar results as the two iterative MTC methods. In the low count study, on the other hand, even though the images were too noisy for visual evaluation, quantitatively, the pGTM+MTC method provided underestimated IMBV of 0.07 while the iMTC method and pGTM+iMTC method provided reasonable estimates of IMBV that were similar to those in the high count study. The pixels with zero values denoted by the blue arrows represented the negative values created by the subtraction operation of the over-estimated spill-in effect.

As demonstrated by quantitative profiles generated from the gated pig study shown in Figure 12, after PVC, the contrast between blood pool and myocardium were improved. The artifact appeared on the lung boundary could be due to the open chest procedure and subsequent non-perfect segmentation and registration of CT template.

As shown previously, the two iMTC methods (Methods E and F) provided similar results. In Figure 13, only the result from Method E is shown, as it yielded slightly better results than Method F in previous evaluations. It can be seen the PVC methods increased blood pool activity and reduced IMBV for all cardiac phases. The standard derivations of blood pool concentrations across all 8 cardiac phases were 1.02%, 1.05%, 0.97% and 0.90% for No PVC, and Methods of pGTM, pGTM+MTC, and iMTC, respectively. Smaller standard deviations indicated more consistent quantification of blood pool across multiple cardiac phases, as the blood pool concentration was not expected to change across different cardiac phases at the state of equilibrium with ^{99m}Tc-RBC labeling. The mean IMBV value across cardiac phases was reduced from 0.18 without PVC to 0.12 with PVC. The true IMBV was unknown in this pig study, and reduced IMBV with PVC was consistent with a reduction in the contribution of "spill-in" counts from the blood pool.

4. Discussion

In this study, we investigated the performance of several anatomical-based partial volume correction approaches for cardiac SPECT imaging over a clinically relevant range of count levels using a dedicated cardiac SPECT/CT system with focused field-of-view. Our simulation results showed that the noise level can have a substantial impact on the

performance of PVC approaches. Compared to conventional methods of pGTM and pGTM +MTC (Methods A and B), the method of pGTM with known blood pool concentration and iterative MTC approaches (Methods C, D, E, and F) provided subjectively superior performance in terms of reduced artifacts, quantitative accuracy, and reproducibility (standard deviation), particularly for noisy data.

We observed that in the ^{99m}Tc-tetrofosmin simulation studies, even though we did not simulate the defect boundary in the anatomical map, mimicking the situation where the perfusion defect was not visible in the contrast-CT data, PVC approaches (Methods C, D, E, and F) effectively reduce the activity bias of the defect and normal myocardium, even in the high noise level cases. The residual errors shown in Figure 10 were likely due to the fact that the residual cross-talks between defect and normal myocardium were not eliminated completely, as we did not have boundary information between normal myocardium and defect in the anatomical information. However, with the boundary information of endocardium and epicardium, quantification of both the myocardium and defect can be improved with PVC.

The proposed iterative PVC approaches are effective in terms of improving accuracy and reproducibility for both ^{99m}Tc-tetrofosmin perfusion imaging and ^{99m}Tc-RBC imaging of IMBV and blood pool activity even at low count levels. These findings are particularly important for dynamic PET and SPECT applications to quantify myocardial blood flow, using other ^{99m}Tc-labeled perfusion tracers or other perfusion agents like Rb-82, NH_3 and thallium-201. During early frames of these dynamic studies, the tracer concentration in the blood pool is typically higher than that of myocardium, similar to the tracer distribution of ^{99m}Tc-RBC study. During later dynamic frames, the tracer concentration is typically higher in the myocardium, similar to the tracer distribution of ^{99m}Tc-tetrofosmin studies. Since the iterative MTC methods were robust for both ^{99m}Tc-tetrofosmin and ^{99m}Tc-RBC imaging even at low count levels, we expect this PVC method can improve the quantitative accuracy for other dynamic cardiac PET and SPECT studies, although this would require further investigation and validation. In existing tracer kinetic modeling, compartmental modeling usually only models the partial volume effect between the blood-pool and myocardium but does not consider contributions from lungs, liver or other organs. Therefore, voxel-by-voxel PVC as a pre-correction step prior to kinetic modeling may be able to improve the quantitative accuracy due to the compensation for spill-in from structures outside the heart.

Comparing Figures 6 and 7, PVC Methods E and F yielded more uniform bias maps for ^{99m}Tc-RBC imaging than for the ^{99m}Tc-tetrofosmin imaging. This indicated that these methods may be more robust in correcting for spill-in dominant images, than for spill-out dominant images when considering the myocardium as the target ROI.

As the MTC approach involved a subtraction operation to correct for spill-in counts (Eq 1), Methods B, E, and F that use MTC would likely generate negative voxel values due to the subtraction in noisy data. In fact, as denoted by the blue arrows in Figure 11, the discrete voxels next to the blood pool with zero activity were caused by this effect. These voxels had negative voxel values and we assigned these voxels to zero for display purpose, albeit

negative voxels were included in quantification. To address the negative voxel value limitation, other PVC approaches that do not involve subtraction operation may be considered. (Yang *et al.*, 1996b; Chan *et al.*, 2013)

The dedicated cardiac SPECT system had a limited FOV of 19 cm in diameter, leading to incomplete sampling for regions outside of the FOV. For our ^{99m}Tc-RBC simulation with typical clinical noise level, the reconstruction mean activities for myocardium, blood pool, lung and liver were respectively 20.0, 95.2, 1.7 and 13.3 without PVC while the true values from NCAT phantom were 15, 100, 2 and 15. The results of organ mean values for other noise levels were similar. With the proposed iterative PVC, regions even outside of the FOV could be recovered quantitatively to 15.0, 99.8, 2.1 and 15.1, for myocardium, blood pool, lung and liver respectively. These results suggested that the proposed PVC methods might be able to increase the effective FOV of dedicated cardiac SPECT system, although this would require further investigation and verification.

In the dog study, all PVC methods led to reduced IMBV for this high count data, indicating the effectiveness of PVC to correct for the overestimation effect. Although no gold standard approach was applied to determine IMBV in the current study, previous studies (Möhlenkamp *et al.*, 2005; Vogel *et al.*, 2005) suggested that the typical IMBV for normal dogs was in the range between 10%–20%, which was consistent with our results after PVC. In future studies, we will validate *in vivo* IMBV quantified by the SPECT/CT approach against *ex vivo* myocardium specimens imaging using ultra-high resolution microCT as the gold standard of IMBV (Malyar *et al.*, 2004).

In the animal study, we used a contrast CT acquired during end-diastolic cardiac phase and end-expiration respiratory phase by temporarily disconnecting the ventilator. During the forward projection and reconstruction of the template, motion blurring effects were not included in this work. Therefore, the PVC corrected images accounted for resolution loss but were still motion blurred. We expect further studies of combining motion correction with PVC will achieve further improved image quality and quantitative accuracy.

In the gated cardiac pig images without PVC, the myocardium wall thickness and blood pool size changed over different phases of the cardiac cycle and resulted in different relative contributions of spill-in and spill-out contaminations, leading to different mean concentrations of blood pool across the phases. In the ideal scenario, PVC methods are expected to provide consistent blood pool quantification across all phases. As shown in Figure 13, however, there were still residual differences across the eight cardiac phases. This may be attributed to the lack of scatter correction, misalignment between CT and SPECT images, and potential inaccuracies in the system model in this study. For dedicated cardiac SPECT with CZT detectors and pinhole collimators, scatter correction methods are not well established due to the unique energy spectrum of pixelated CZT detectors. Incorporating scatter correction into PVC to further improve quantitative accuracy needs further investigation.

In this work, the forward projector used to generate the projection data was identical to the forward projector used in the reconstruction. We expect this exact match between the

simulation model and reconstruction could lead to the best possible performance of each PVC method but expect that the results of the comparisons among various PVC methods would still hold. That being said, a different forward projector model is needed in future studies to allow the investigation of various PVC methods in a more realistic manner.

In animal studies, we did not perform cross-calibrated blood sample well counting to obtain true blood pool activity to guide PVC Methods C and D, which will be performed in future studies.

The CT segmentation and mismatch between SPECT and CT could also introduce errors in the large animal studies. In this study, the segmentation and registration on contrast CT data were performed manually, which may not be consistent and reproducible. However, the segmentation and registration were the same for all compensation methods. Therefore, even though there might be a systematic bias, the relative comparison of the methods would be less affected by errors in registration or segmentation. Particularly in the dog study, due to the open chest surgical procedure and anticoagulation, there was some mild bleeding and accumulation of ^{99m}Tc-RBCs within the chest cavity throughout the study. Therefore, a mismatch could exist between the contrast CT and SPECT images, which were acquired at two time points approximately 30 minutes apart. In future studies, there might be an advantage to using automatic or semi-automatic segmentation approaches to improve the accuracy and consistency of the segmentation.

In this study, we investigated various PVC approaches for cardiac perfusion SPECT with ^{99m}Tc-tetrofosmin and ^{99m}Tc-RBC imaging. However, we expect that additional PVC methods, in particular the iterative PVC method, could also be applied for future SPECT and PET investigations targeting various molecular processes.

5. Conclusions

In this study, we have investigated several PVC approaches for dedicated cardiac SPECT/CT imaging with both ^{99m}Tc-tetrofosmin and ^{99m}Tc-RBC tracers. Our proposed iMTC (iterative PVC methods) and pGTM methods with known blood pool concentration provide superior performance than conventional pGTM and MTC methods, particularly for the low count data that can be obtained from low-dose protocols, gated studies, and dynamic applications.

Acknowledgments

This work was supported by NIH grants R01HL123949, R01HL113352, T32HL098069, and 1S10RR02555, and a research contract from GE Healthcare.

References

Bocher M, Blevis IM, Tsukerman L, Shrem Y, Kovalski G, Volokh L. A fast cardiac gamma camera with dynamic SPECT capabilities: design, system validation and future potential. EUR J NUCL MED MOL I. 2010; 37:1887–1902.

Chan C, Dey J, Sinusas A, Liu C. Improved image reconstruction for dedicated cardiac SPECT with truncated projections. J NUCL MED. 2012; 53(Supplement 1):105. (abstract).

Chan, C.; Liu, H.; Grobshtein, Y.; Stacy, M.; Sinusas, AJ.; Liu, C. Simultaneous Partial Volume Correction and Noise Regularization for Cardiac SPECT/CT; Nuclear Science Symposium and Medical Imaging Conference (NSS/MIC), 2013 IEEE; 2013. p. 1-6.

Du Y, Tsui BM, Frey EC. Partial volume effect compensation for quantitative brain SPECT imaging. Medical Imaging, IEEE Transactions on. 2005; 24:969–976.

Erlandsson K, Buvat I, Pretorius PH, Thomas BA, Hutton BF. A review of partial volume correction techniques for emission tomography and their applications in neurology, cardiology and oncology. PHYS MED BIOL. 2012; 57:R119. [PubMed: 23073343]

Erlandsson K, Wong AT, van Heertum R, Mann JJ, Parsey RV. An improved method for voxel-based partial volume correction in PET and SPECT. NEUROIMAGE. 2006; 31:T84.

Frouin V, Comtat C, Reilhac A, Gr E, Goire M. Correction of partial-volume effect for PET striatal imaging: fast implementation and study of robustness. J NUCL MED. 2002; 43:1715–1726. [PubMed: 12468524]

Garcia EV, Faber TL, Esteves FP. Cardiac dedicated ultrafast SPECT cameras: New designs and clinical implications. J NUCL MED. 2011; 52:210–217. [PubMed: 21233190]

He X, Frey EC, Links JM, Gilland KL, Segars WP, Tsui BM. A mathematical observer study for the evaluation and optimization of compensation methods for myocardial SPECT using a phantom population that realistically models patient variability. Nuclear Science, IEEE Transactions on. 2004; 51:218–224.

Hoetjes NJ, van Velden FH, Hoekstra OS, Hoekstra CJ, Krak NC, Lammertsma AA, Boellaard R. Partial volume correction strategies for quantitative FDG PET in oncology. EUR J NUCL MED MOL I. 2010; 37:1679–1687.

Kennedy JA, Israel O, Frenkel A. 3D iteratively reconstructed spatial resolution map and sensitivity characterization of a dedicated cardiac SPECT camera. J NUCL CARDIOL. 2014; 21:443–452. [PubMed: 24429938]

Liu C, Chan C, Stacy M, Miller K, Bregasi A, Dione D, Zhuang Z, Sinusas A. Feasibility of Quantifying Intramyocardial Blood Volume using SPECT/CT. Society of Nuclear Medicine Annual Meeting Abstracts, 2013. 2013; 54(Supplement 2):404.

Malyar NM, Gössl M, Beighley PE, Ritman EL. Relationship between arterial diameter and perfused tissue volume in myocardial microcirculation: a micro-CT-based analysis. AM J PHYSIOL-HEART C. 2004; 286:H2386–H2392.

Möhlenkamp, S.; Schmermund, A.; Kantor, B.; Erbel, R.; Ritman, EL. CT of the heart. Humana Press; 2005. Imaging Intramyocardial Microcirculatory Function Using Fast Computed Tomography; p. 195-206.

Muller-Gartner HW, Links JM, Prince JL, Bryan RN, McVeigh E, Leal JP, Davatzikos C, Frost JJ. Measurement of radiotracer concentration in brain gray matter using positron emission tomography: MRI-based correction for partial volume effects. J Cereb Blood Flow Metab. 1992; 12:571–583. [PubMed: 1618936]

Pretorius PH, King MA. Diminishing the impact of the partial volume effect in cardiac SPECT perfusion imaging. MED PHYS. 2008; 36:105–115. [PubMed: 19235379]

Rousset OG, Ma Y, Evans AC, et al. Correction for partial volume effects in PET: principle and validation. J NUCL MED. 1998; 39:904–911. [PubMed: 9591599]

Segars WP, Lalush DS, Tsui B. Development of an interactive software application to model patient populations in the 4D NURBS-based cardiac torso phantom. 2000:20–51.

Soret M, Koulibaly PM, Darcourt J, Hapdey SEB, Buvat IEN. Quantitative accuracy of dopaminergic neurotransmission imaging with 123I SPECT. J NUCL MED. 2003; 44:1184–1193. [PubMed: 12843235]

Thomas BA, Erlandsson K, Modat M, Thurfjell L, Vandenberghe R, Ourselin S, Hutton BF. The importance of appropriate partial volume correction for PET quantification in Alzheimer's disease. EUR J NUCL MED MOL I. 2011; 38:1104–1119.

Vogel R, Indermühle A, Reinhardt J, Meier P, Siegrist PT, Namdar M, Kaufmann PA, Seiler C. The quantification of absolute myocardial perfusion in humans by contrast echocardiographyalgorithm and validation. J AM COLL CARDIOL. 2005; 45:754–762. [PubMed: 15734622]

Wienhard K, Schmand M, Casey ME, Baker K, Bao J, Eriksson L, Jones WF, Knoess C, Lenox M, Lercher M, et al. The ECAT HRRT: performance and first clinical application of the new high resolution research tomograph. Nuclear Science, IEEE Transactions on. 2002; 49:104–110.

Yang J, Huang SC, Mega M, Lin KP, Toga AW, Small GW, Phelps ME. Investigation of partial volume correction methods for brain FDG PET studies. Nuclear Science, IEEE Transactions on. 1996a; 43:3322–3327.

Yang J, Huang SC, Mega M, Lin KP, Toga AW, Small GW, Phelps ME. Investigation of partial volume correction methods for brain FDG PET studies. Nuclear Science, IEEE Transactions on. 1996b; 43:3322–3327.

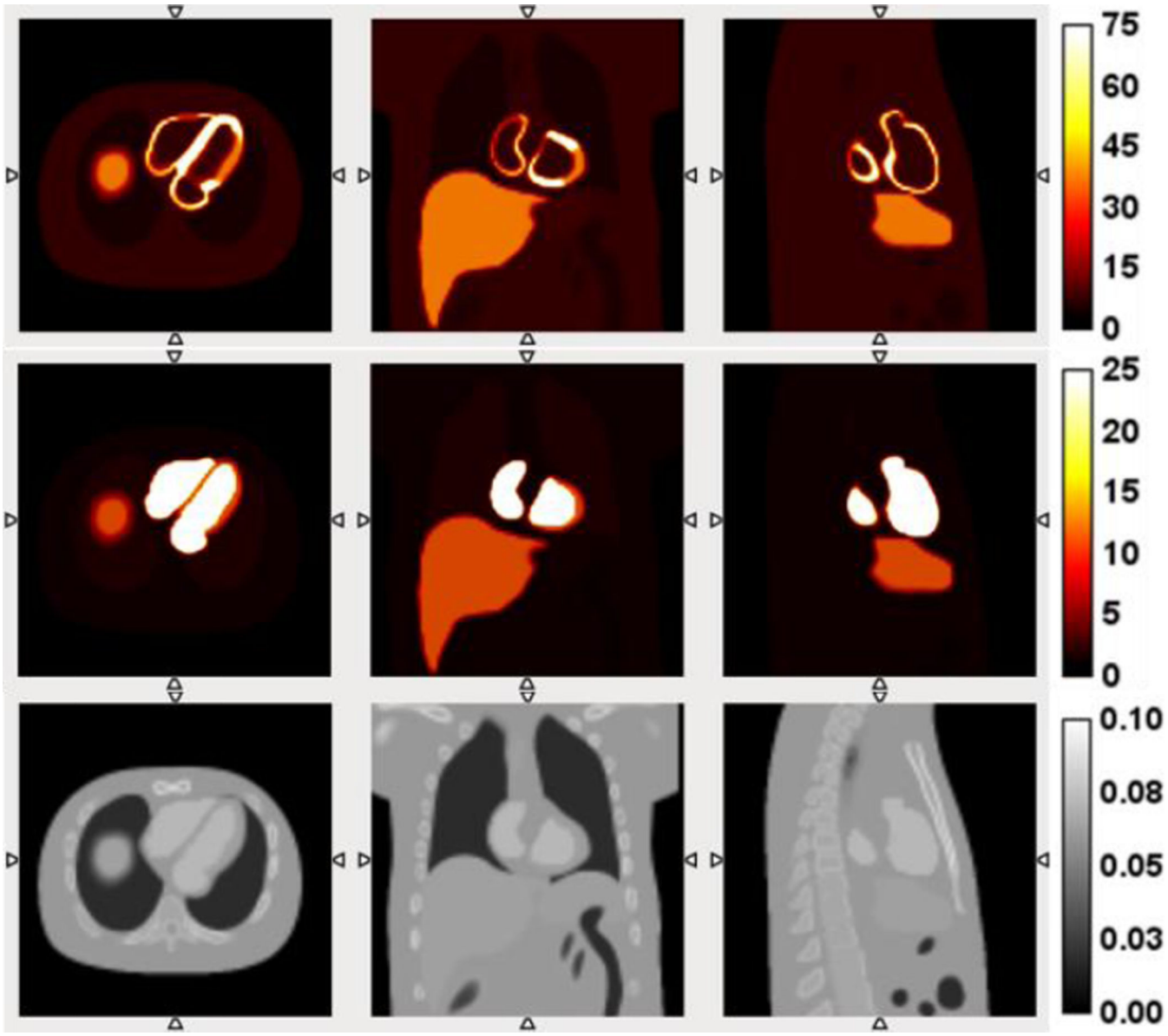

Figure 1.

NCAT phantom slices for simulation of the distribution of ^{99m}Tc-tetrofosmin (top row), ^{99m}Tc-RBCs (middle row) and corresponding contrast CT slices (bottom row). From left to right: transverse view, coronal view, and sagittal view.

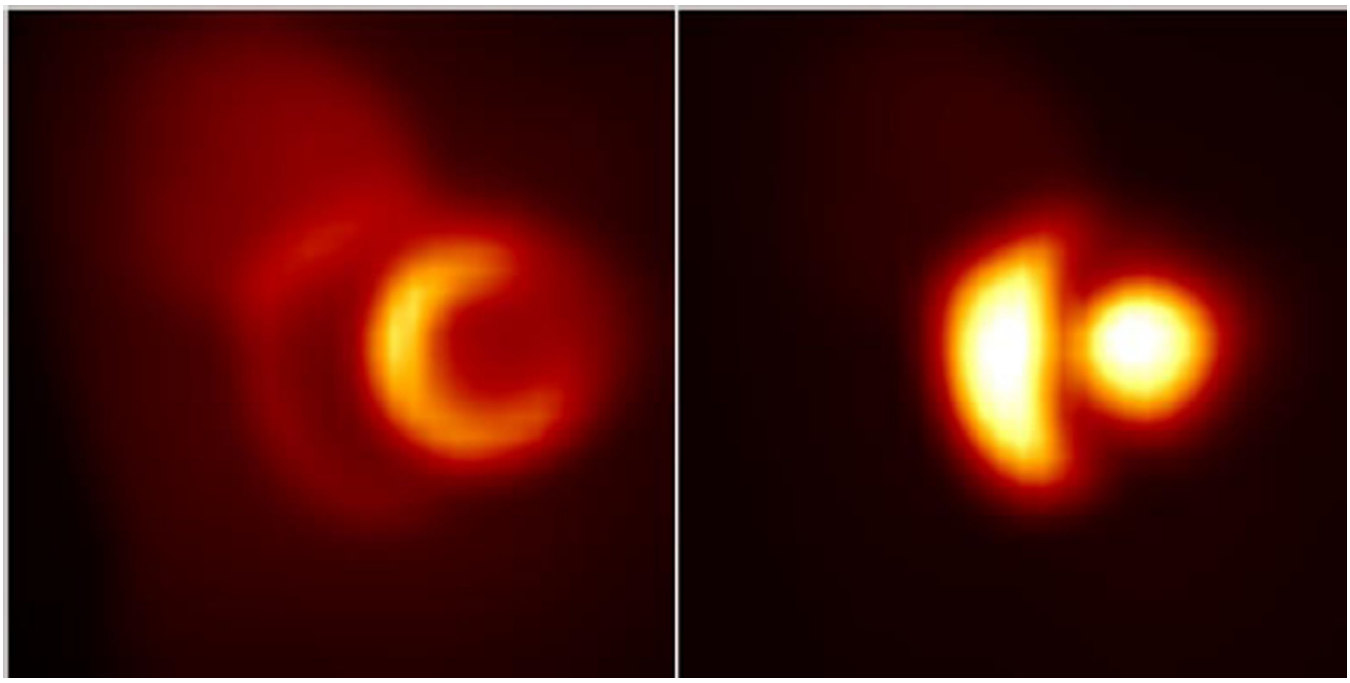

Figure 2.
Sample noise-free projections of NCAT phantom simulating ^{99m}Tc-tetrofosmin (left) and ^{99m}Tc-RBCs (right)

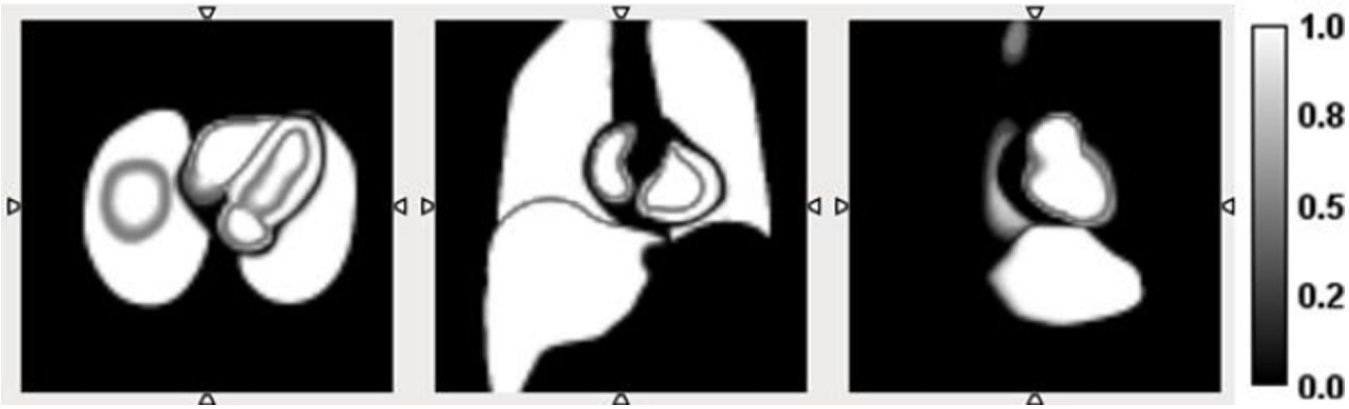

Figure 3.
Sample slices of the segmented templates of four regions with tissue fraction, illustrated by grey gradient. From left to right: transverse view, coronal view, sagittal view.

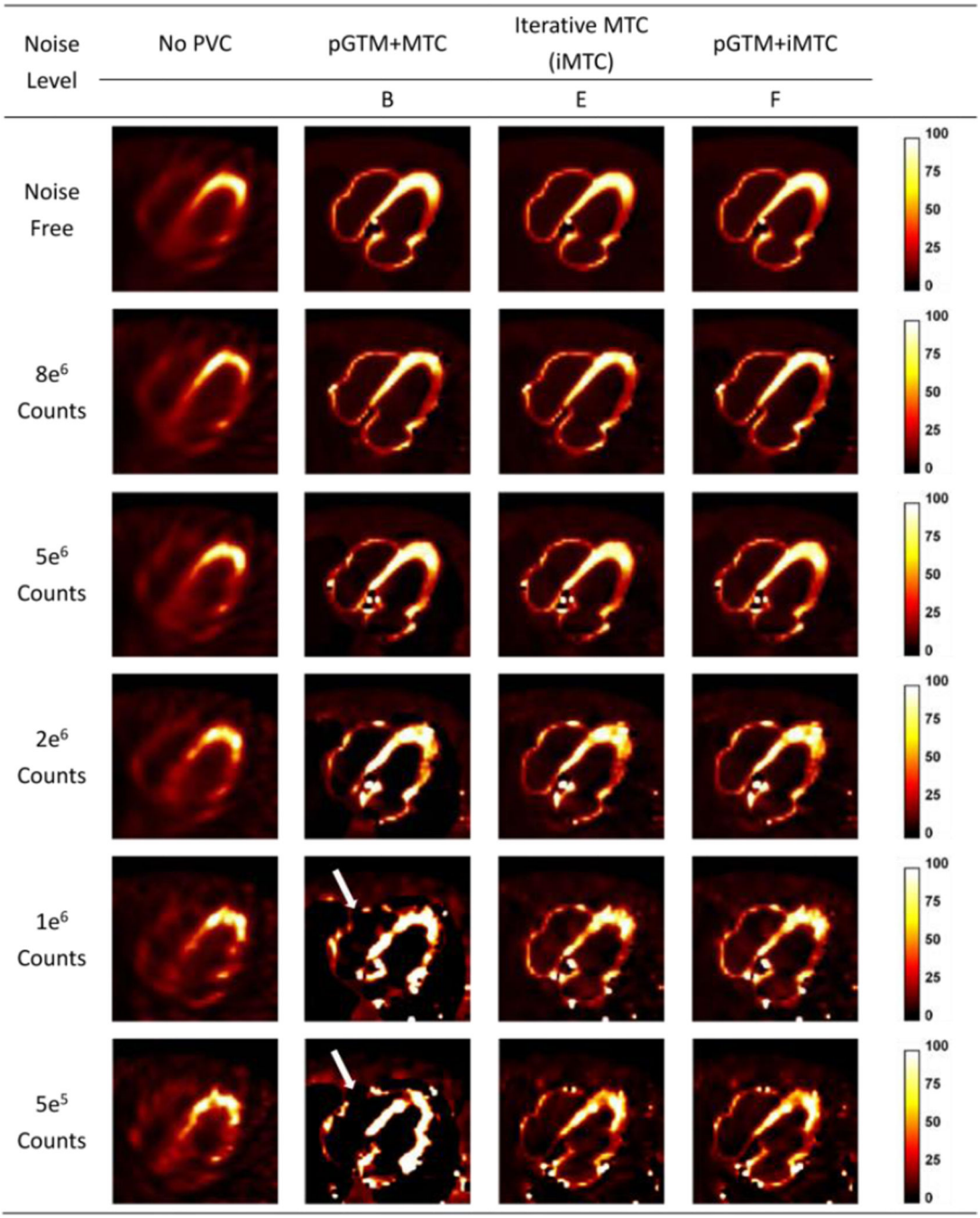

Figure 4.

Sample slices of NCAT phantom simulation at different count levels without and with different PVC approaches for ^{99m}Tc-tetrofosmin simulations. Artifacts appeared at lower count levels with method B, as pointed out by the white arrows.

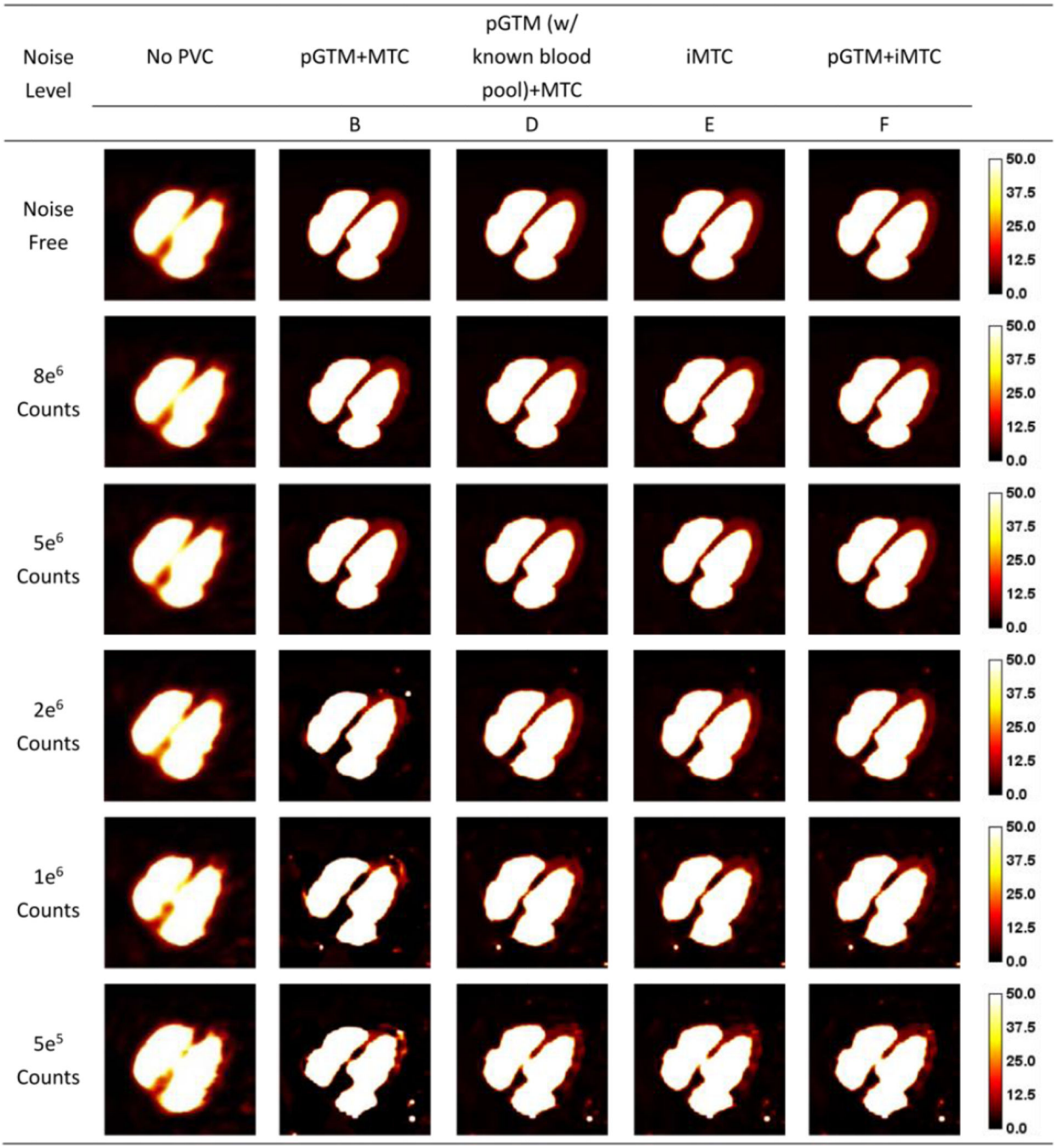

Figure 5.
Sample slices of NCAT phantom at different count levels without and with different PVC approaches for ^{99m}Tc-RBC simulations.

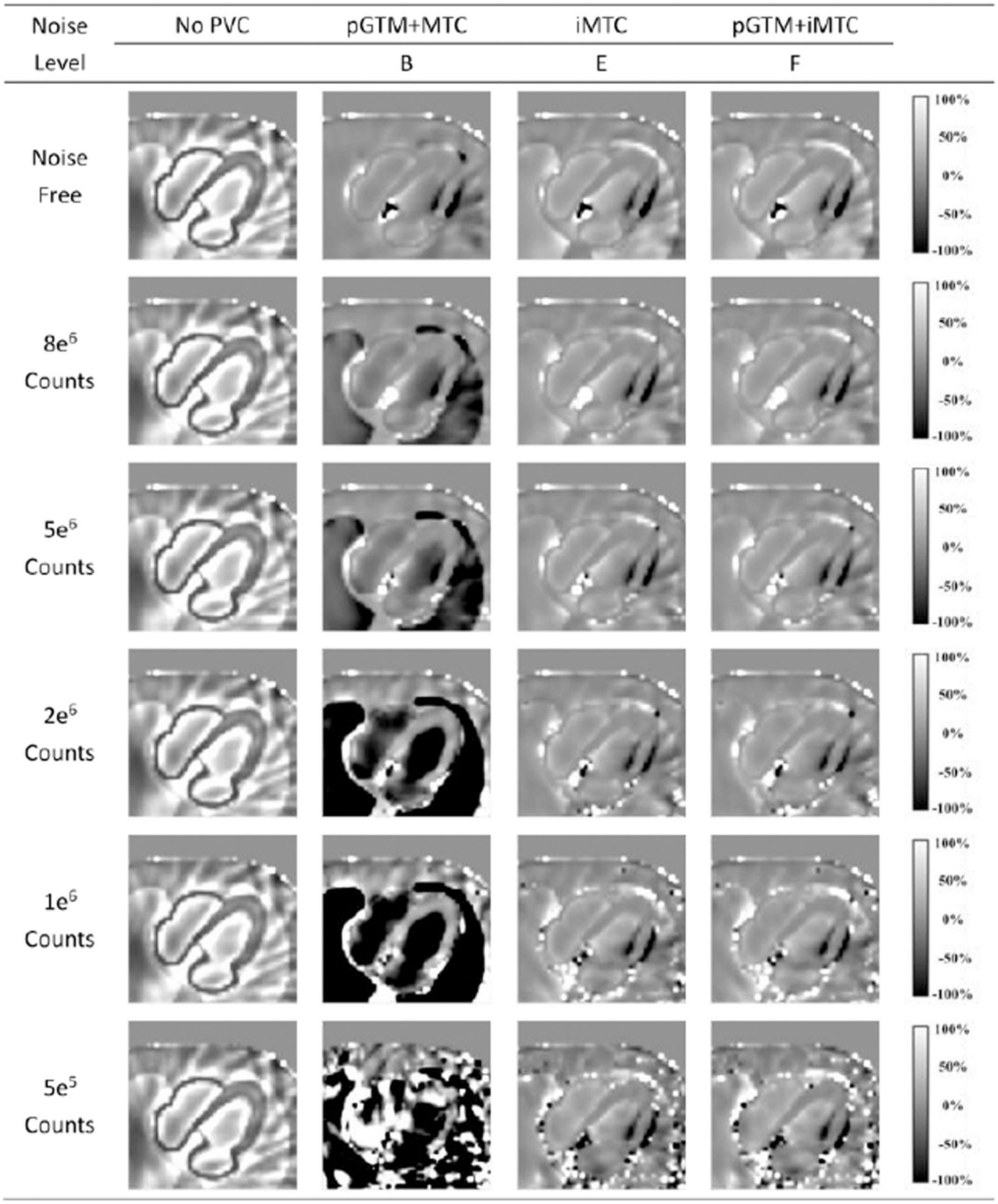

Figure 6.

Normalized bias images for different count levels without and with different PVC approaches for the ^{99m}Tc-tetrofosmin simulations.

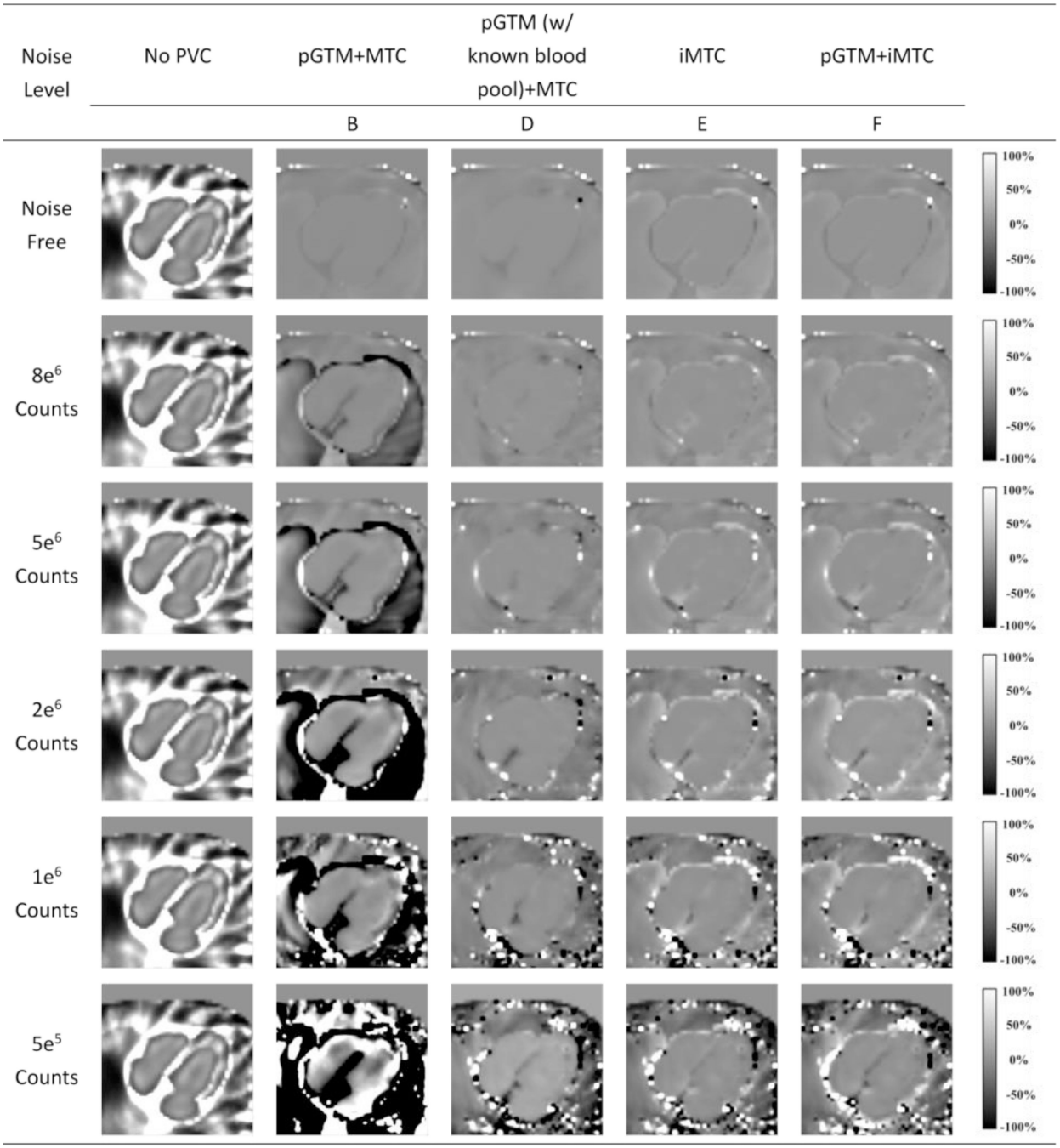

Figure 7.

Normalized bias images for different count levels without and with different PVC approaches for the ^{99m}Tc-RBC simulations.

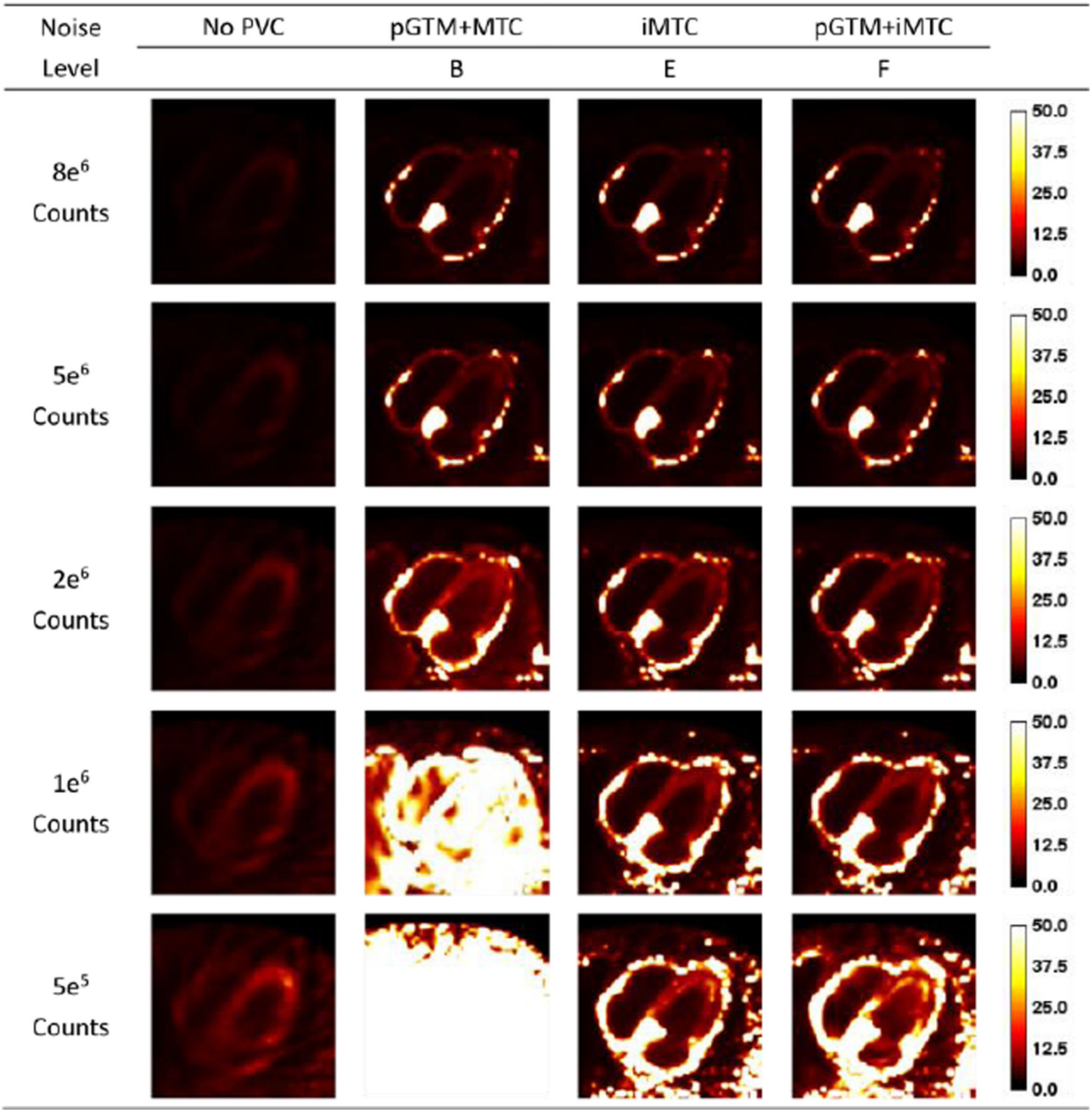

Figure 8.
Standard derivation images for different count levels without and with different PVC approaches for the ^{99m}Tc-tetrofosmin simulations.

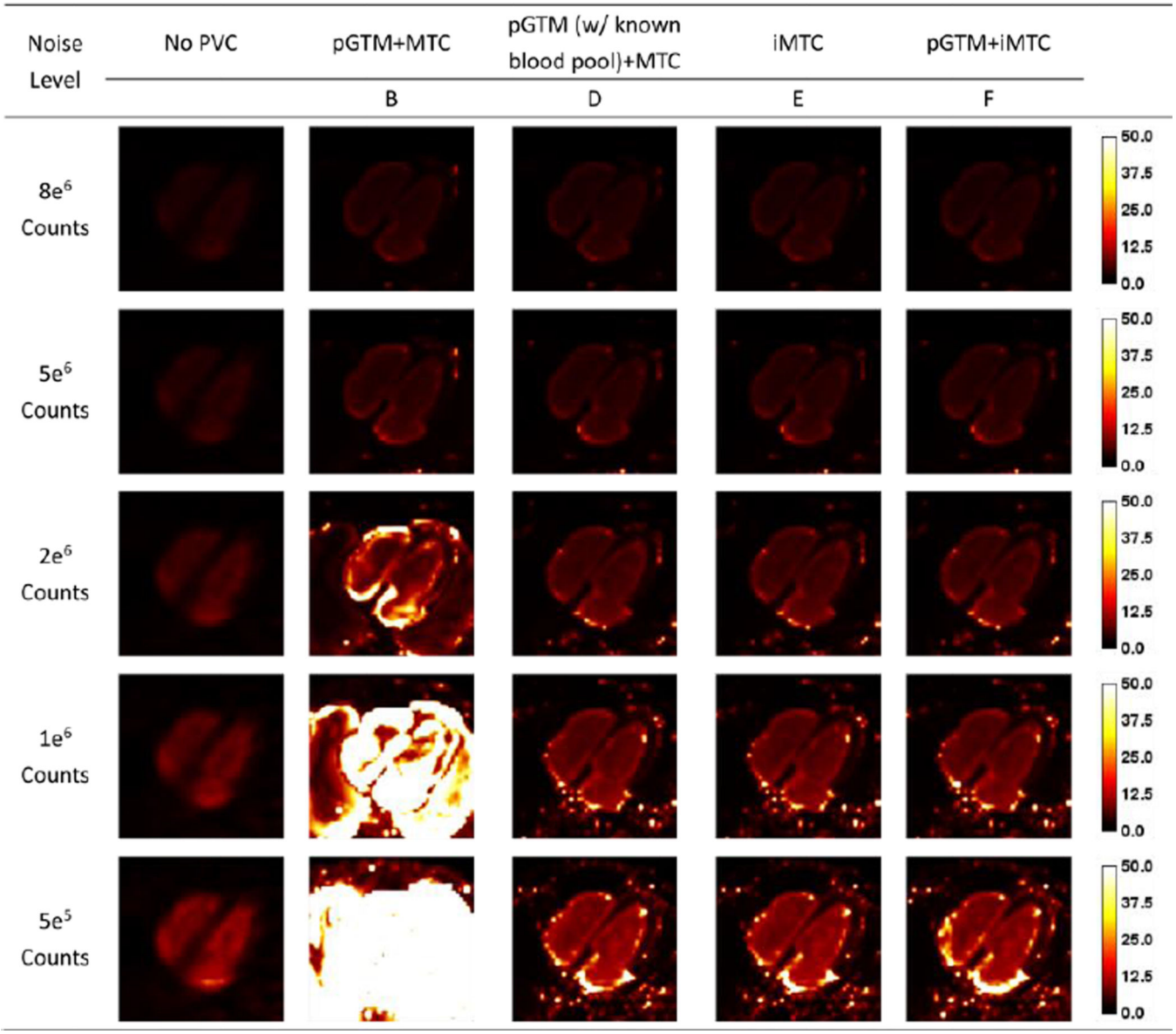

Figure 9.

Standard derivation images for different count levels without and with different PVC approaches for the ^{99m}Tc-RBC simulations.

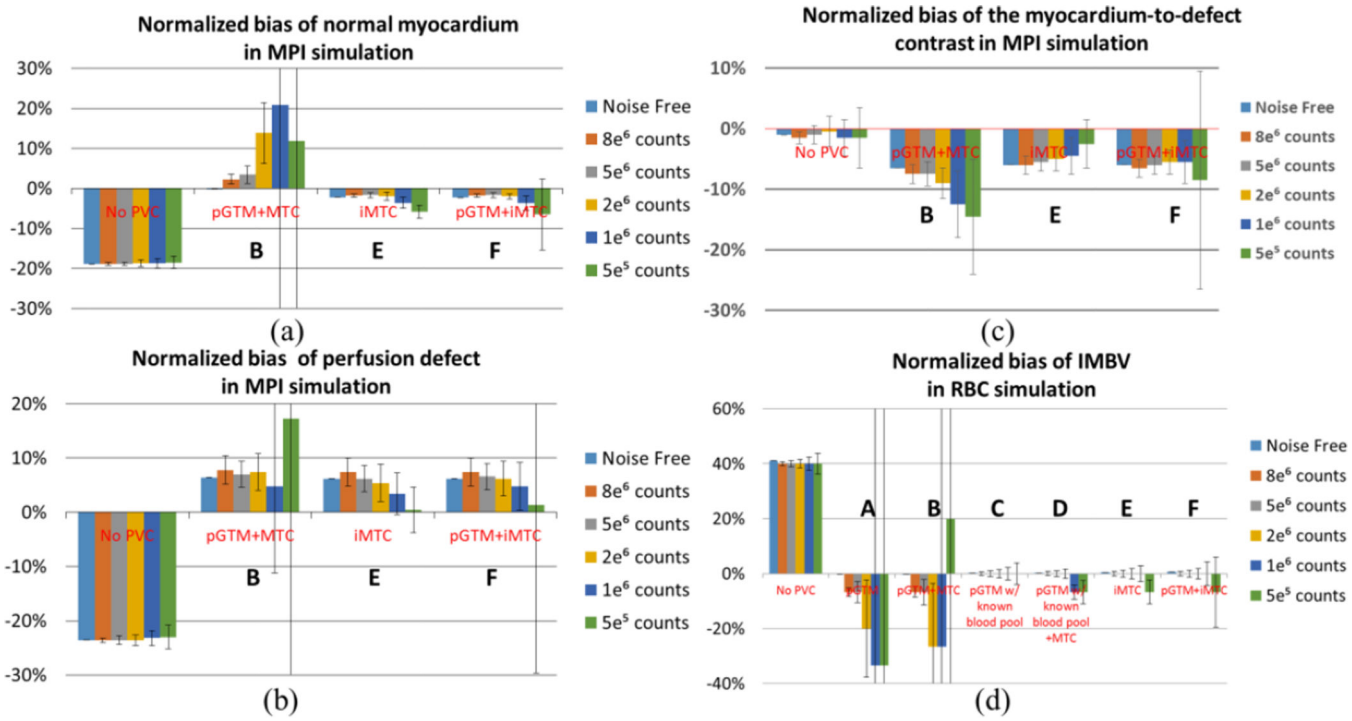

Figure 10.

Normalized ROI bias for normal myocardium, perfusion defect and the myocardium-to-defect contrast for the ^{99m}Tc-tetrofosmin simulation and IMBV of the entire myocardium for the ^{99m}Tc-RBC simulations with a 15% true IMBV. The error bar represents standard deviations of IMBV across 50 noise realizations. The error bar for $5e^5$ counts for pGTM +MTC and pGTM+iMTC are more than one hundred percent, so we did not include the full range in the plot.

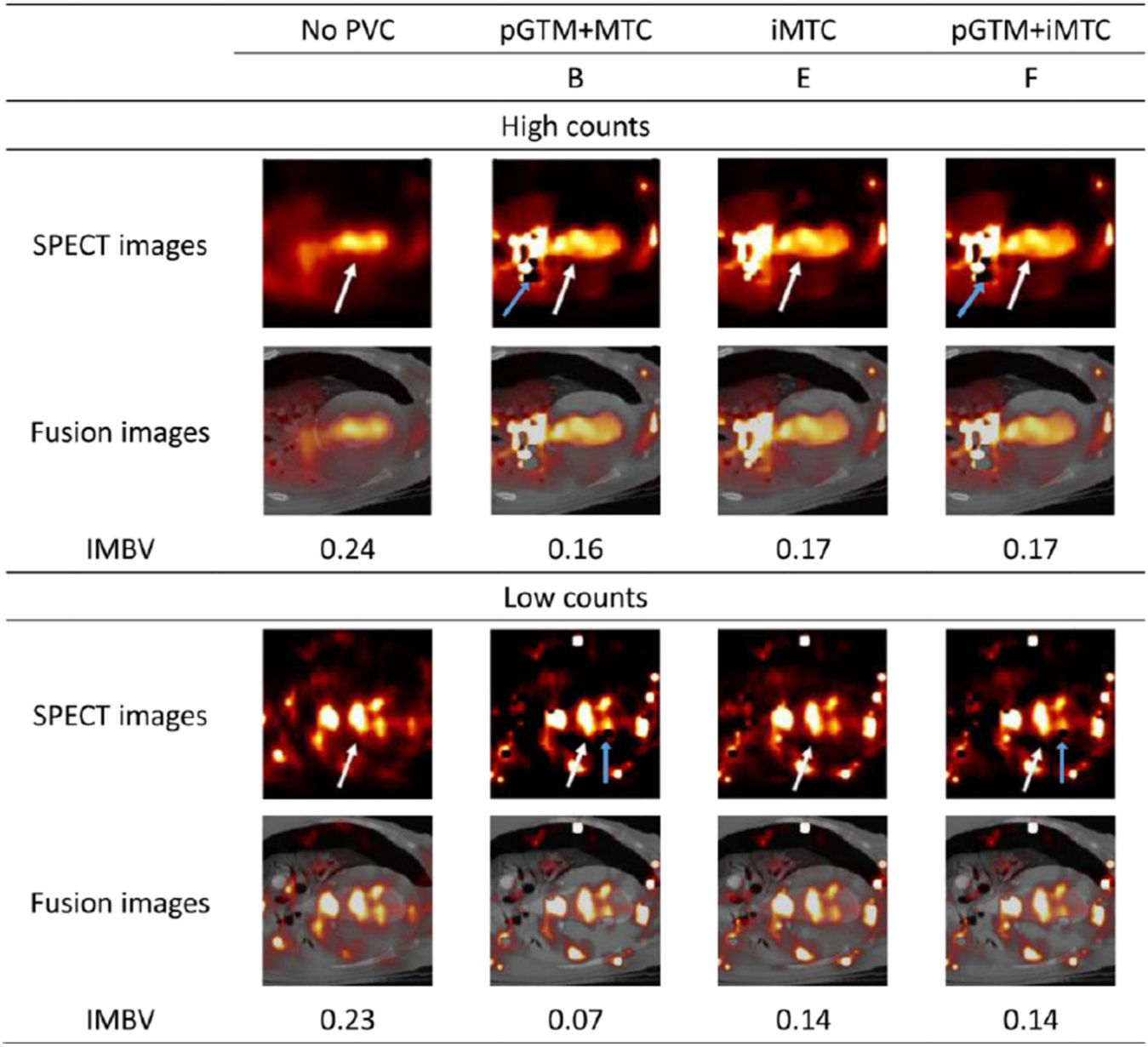

Figure 11.

Sample images without and with different PVC approaches of the dog study with high and low count levels. The white arrows denote the boundary between myocardium and blood pool. The blue arrows denote the pixels with zero values.

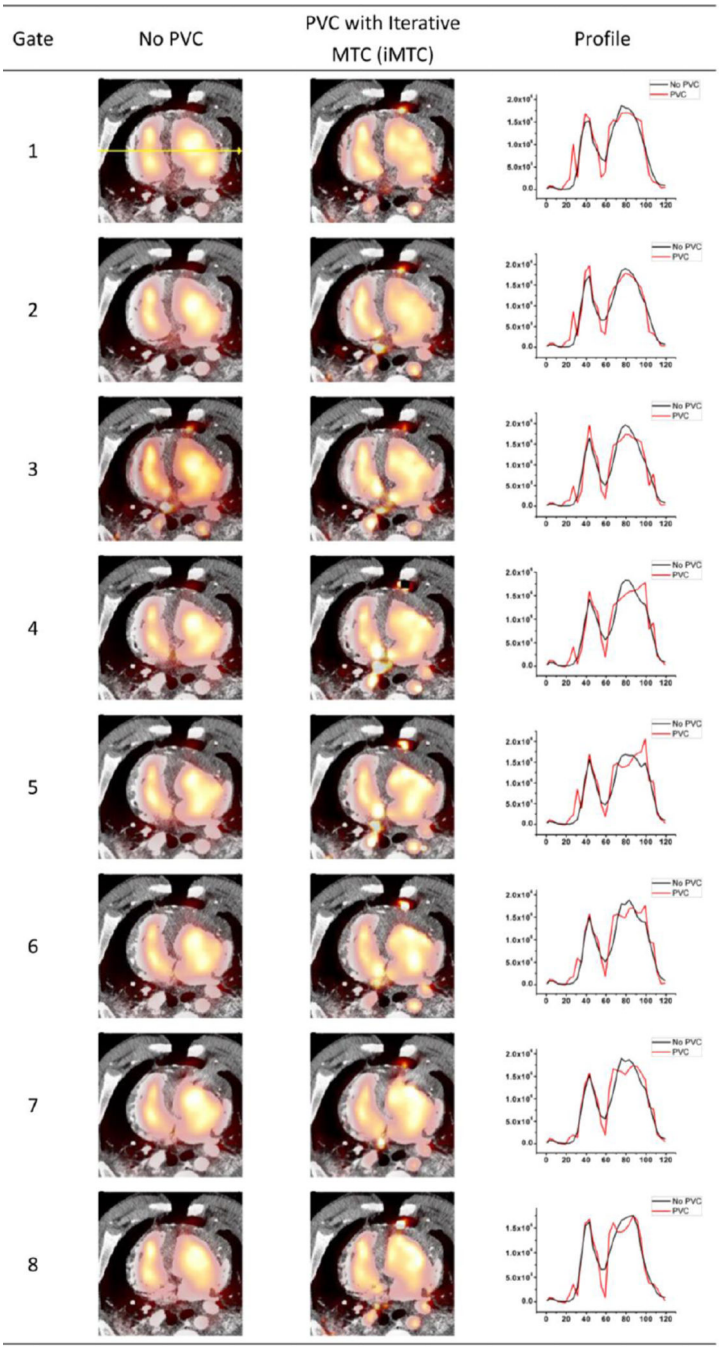

Figure 12.

Sample slices for the gated pig study without and with PVC using iMTC (Method E) and corresponding horizontal profiles through the heart from each of the 8 cardiac phases. Black profiles represent no PVC results while the red profiles represent the PVC results.

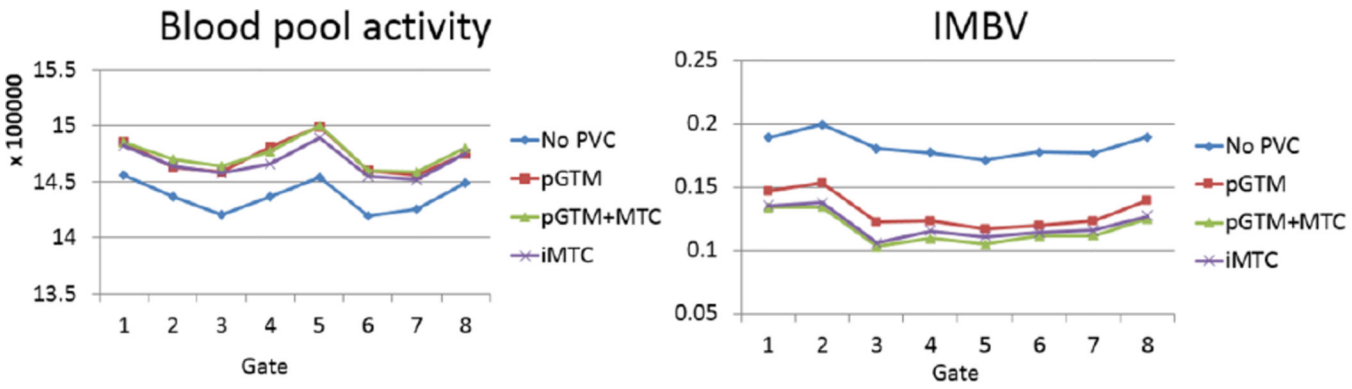

Figure 13.

Blood pool activity (defined as the mean value within the entire blood pool) and IMBV are plotted across the cardiac phases for each of the different PVC approaches for the gated pig study.

Table 1

Summary of all the PVC methods used in this study.

Method index	PVC Method	Abbreviation	Detail and Features
A	Perturbation Geometry Transfer Matrix	pGTM	Detail was given in (Du *et al.*, 2005). It only provided mean activity of each region.
B	pGTM method followed by the MTC method	pGTM+MTC	The pGTM approach was used to obtain region mean activities first and MTC approach was used for subsequent voxel-by-voxel correction.
C	pGTM with known concentration in blood pool	pGTM w/known blood pool	For RBC tracer, it was feasible to obtain and count blood samples at equilibrium state to serve as the true tracer concentration in the blood pool region. pGTM estimated the mean activities in regions other than the blood pool.
D	pGTM with known concentration in blood pool, followed by the MTC method	pGTM (w/known blood pool)+MTC	The prior information of true blood pool concentration may subsequently improve the quantification on the voxel-by-voxel basis PVC using MTC.
E	Iterative MTC	iMTC	Correcting for "spill-in" counts required accurate mean activities of each region, which were also affected by partial volume effect. Even though pGTM may provide accurate mean activities for high count data, as demonstrated by our data below, pGTM failed to provide accurate region activity in low count data. Here we proposed an iterative approach that repeatedly applied MTC approach to the original reconstructed image without the prior pGTM step. After each iteration, the mean activities of each region were recalculated and were used to guide MTC correction for the next iteration.
F	pGTM followed by iterative MTC	pGTM+iMTC	We would like to investigate if applying pGTM as initial estimate could improve the results of iterative MTC.